

# Ablation thresholds in ultrafast laser micro-machining of common metals in air

Paul Mannion\*, Jonathan Magee, Edward Coyne, Gerard M. O'Connor  
National Centre for Laser Applications, National University of Ireland, Galway, Ireland

## ABSTRACT

In the current work ablation of metal targets in air with femtosecond laser pulses is studied. The laser pulses used for the study were 775 nm in wavelength, 150 fs in pulse duration and the repetition rate was 100 Hz. Ablation thresholds have been measured for a number of metals including stainless steel (0.1600 J/cm<sup>2</sup>), niobium (0.1460 J/cm<sup>2</sup>), titanium (0.1021 J/cm<sup>2</sup>) and copper (0.3529 J/cm<sup>2</sup>). The ablation depth per pulse was measured for laser pulse fluences ranging from the ablation threshold (of most metals) ~ 0.1 J/cm<sup>2</sup> up to 10 J/cm<sup>2</sup>. It has been shown previously that there are two different ablation regimes.<sup>1</sup> In both cases the ablation depth per pulse depends logarithmically on the laser fluence. Whilst operating in the first ablation regime the ablation rate is low and is dependant on the optical penetration depth,  $\alpha^{-1}$ . While in the second ablation regime the ablation rate is greater and is characterized by the "electron heat diffusion length" or the "effective heat penetration depth",  $l$ . In the present study good qualitative agreement in the ablation curve trends was observed with the data of other authors, e.g. Nolte et al (1997).<sup>1</sup>

**Keywords:** femtosecond pulse laser, ablation threshold, micromachining, laser materials processing, metals.

## 1. INTRODUCTION

The rapid development of ultra-fast laser systems has prompted many research groups to investigate their application in real world laser materials processing (LMP).<sup>2,3,4,5,6</sup>

Ultrashort pulsed laser ablation has become a very active area of research in recent years. It is definitely one of the most industrially driven technologies to have arisen from femtosecond laser applications because it allows materials processing of practically any material with extremely high precision and minimal collateral damage. There are obvious areas where such a capability would be very useful, most notably for the fabrication of semiconductor devices and certain medical devices, which could be directly manufactured without the need for any post processing i.e. electro-polishing.

Ultrashort pulsed laser ablation presents many challenges because the underlying physics is completely different from that in conventional nanosecond pulsed laser ablation.<sup>7,8</sup> Processing with ultrashort laser pulses has many advantages over longer pulsed lasers (pulses longer than a few tens of picoseconds). By depositing the laser energy into the electrons of the material on a time-scale short compared with the transfer time of this energy to the bulk of the material, the ablation efficiency is improved and the ablation threshold is reduced and more well defined. Using ultrashort pulses causes a direct solid-vapour transition at high enough intensities. Obviously this leads to a strong reduction of material melting which increases the repeatability of the machining processing unlike conventional laser processing where repeatability is hindered by the randomness of the melting process. The fact that the molten phase is practically absent also reduces shock and thermal stress, which means that the Heat Affected Zone (HAZ) around the machined feature is minimized. Another advantage is the absence of a plasma shielding effect because the pulses are so short.

In this paper there are two separate parts. In the first part, quantitative results are obtained for the ablation threshold fluences of stainless steel, copper, titanium and niobium using a method employed by J. Bonse et al<sup>9</sup>, which is explained in detail in the results section. The second part of the paper deals with ablation rates of the above metals and graphs of the ablation rates are presented. These graphs are intended to show qualitative agreement with other authors,<sup>1</sup>

---

\* Email: pmannion@nuigalway.ie; Tel.: 353-91-750469 (ext. 2515); Fax 353-91-750594.

especially with regards to the existence of two distinct ablation regimes. In order to qualitatively explain the phenomena a brief theoretical discussion is required.

### 1.1 Theoretical Discussion

Electron and phonon dynamics following irradiation with ultrashort laser pulses govern the rise in temperature of the electrons and the lattice and hence any phase transitions (e.g. solid-vapour), which take place in the solid. Electron dynamics have been widely investigated using a technique known as “pump-probe spectroscopy”.<sup>10,11,12</sup> The technique employs an ultrashort excitation (“pump”) pulse, which heats the electrons at the metal surface. Changes in the optical reflectivity are related to the electron dynamics and are monitored with a second (“probe”) pulse. The findings of these investigations can be summarized as follows:

- Upon irradiation with ultrashort laser pulses the laser energy is first absorbed by the free electrons in a metal, owing to the inverse Bremsstrahlung.<sup>1</sup>
- There follows a rapid thermalization within the electron gas to a Fermi-Dirac temperature distribution which occurs by electron-electron scattering.<sup>10</sup>
- Because of the relatively small electronic heat capacity of metals (1 to 2 orders of magnitude smaller than the lattice heat capacity), peak electronic temperatures of thousands of K above the relatively cold lattice and the equilibrium melting temperature can be achieved.
- Heat is transferred into the target by the diffusive transport of thermalized electrons and the ballistic transport of nonthermalized electrons. This sometimes leads to energy penetrating to a depth that is greater than the optical penetration depth, known as the “electron heat diffusion length” or the “effective heat penetration depth”,  $l$ .
- While this is taking place heat is being transferred from the electronic system to the lattice by means of electron-phonon coupling.
- The rate of heat transfer by electron-phonon coupling is determined by the electron-phonon coupling constant,  $g$ . The greater,  $g$ , the greater the rate of heat transfer between the electrons and the lattice and hence the faster the thermalization between the electronic and lattice subsystems.
- When the electronic and lattice subsystems have thermalized both the diffusive transport of thermalized electrons and the ballistic transport of nonthermalized electrons stops. Hence the “electron heat diffusion length” depends on the strength of the electron-phonon coupling constant,  $g$ .<sup>13</sup>
- It is possible to say that for ultrashort excitation the penetration depth of the absorbed energy into the lattice, at the time when the maximum surface temperature is reached (i.e. when the electronic and lattice subsystems have thermalized) is given by the diffusion length of the hot excited electrons, which are not in thermal equilibrium with the lattice during the first picoseconds after irradiation. This is in contrast to ns-laser damage, where the penetration depth of the absorbed energy in the lattice is given by the thermal diffusion length of the solid with electrons and lattice in thermal equilibrium.<sup>12</sup>

### 1.2 The two temperature model

The one dimensional two temperature model has been used extensively in order to explain what happens during ablation.<sup>1,14</sup> In this model the electron and lattice subsystems are treated as two separate heat baths with temperatures  $T_e$  and  $T_l$ . One has to assume that electron thermalization is very fast compared to the pulse length in order to justify the use of an electronic temperature but this has been shown to be the case.<sup>10</sup> The two main equations of the model are as follows:

$$C_e(T_e) \frac{\delta T_e}{\delta t} = -\frac{\delta}{\delta z} \left( k_e \frac{\delta T_e}{\delta z} \right) - g(T_e - T_l) + S(z, t), \quad (1)$$

$$C_l(T_l) \frac{\delta T_l}{\delta t} = g(T_e - T_l). \quad (2)$$

$C_e$  and  $C_l$  are the electronic and lattice heat capacities respectively. Equation (1) describes electronic heat diffusion with the first term where,  $k_e$ , is the electron thermal conductivity. The second term describes electron-phonon coupling and the third term describes the heating of the electrons by the laser pulse,  $S(z,t)$  is the absorbed laser energy density per unit time (i.e the source term). The heat diffusion through the lattice is neglected in the second equation because heat diffusion occurs much more rapidly through the electron gas than through the lattice phonons because of the aforementioned difference between the heat capacities of the electrons and the lattice.

Nolte et al<sup>1</sup> have shown, using the above model, that there are two separate ablation regimes, i.e. two separate logarithmic dependences of the ablation rate on the peak laser fluence can be identified. For low peak laser fluences ( $\phi_0 < 1\text{J/cm}^2$ ), the ablated depth per pulse (DPP),  $L$ , can be described by the well known expression

$$L \approx \alpha^{-1} \ln(\phi_0 / \phi_{th}^\alpha), \quad (3)$$

where  $\alpha^{-1}$  is the optical penetration depth and  $\phi_0^\alpha$  is the ablation threshold for the low fluence regime.

At higher peak fluences ( $\phi_0 > 1\text{J/cm}^2$ ) the second logarithmic dependence appears and can be described by the expression

$$L \approx l \ln(\phi_0 / \phi_{th}^l). \quad (4)$$

This regime is characterized by the “electron heat diffusion length”,  $l$ , and the ablation threshold for the higher fluence regime,  $\phi_0^l$ .

In order to understand why the two regimes are present one must make use of the fact that the dynamics of the electron heating and cooling process are non-linear. At electronic temperatures much higher than the Fermi temperature,  $T_F$ ,

$$T_F = E_F / k_B, \quad (5)$$

(where  $E_F$  is the Fermi energy and  $k_B$  is the Boltzman constant) the electronic heat capacity is constant,

$$C_e = 3N_e k_B / 2, \quad (6)$$

(where  $N_e$  is the electron density) but the electron thermal conductivity,  $k_e$ , grows with the electron temperature,  $T_e$ , as

$$k_e \sim T_e^{\frac{5}{2}}. \quad (7)$$

While the electrons and the lattice are not at thermal equilibrium electronic heat conduction is taking place. The higher the temperature reached by the electrons (i.e. the higher the incident laser fluence) the greater the rate of electronic heat conduction according to (7) and (1). Also the higher the temperature reached by the electrons, the longer it takes for the electronic subsystem to come to thermal equilibrium with the lattice (1), thus allowing more time for electronic heat conduction to take place at its elevated rate. Thus whilst operating at higher fluences the ablation is characterized by the “electron heat diffusion length”,  $l$ .

At lower laser fluences the density of hot electrons is lower and the rate of electronic heat conduction is also lower. The electrons and lattice reach thermal equilibrium faster because of the smaller difference in electronic and lattice temperatures (1), thus allowing less time for electronic conduction at its reduced rate. Therefore the amount of energy transfer out of the optical skin depth and into the target is negligible and the ablation is characterized by the optical penetration depth.

## 2. EXPERIMENTAL

The ablation of all metals was performed using the direct focusing technique under atmospheric pressure with a commercially available titanium-sapphire laser (Clark MXR, CPA2001) equipped with a chirped pulse amplification system. The laser emits pulses of linearly polarized light at a central wavelength of 775nm. The pulse width can be changed by varying the distance between the pulse compressor gratings. The pulses used for the experiments presented here were all of 150fs in duration. The pulse width was measured by means of a second order autocorrelator by fitting the pulses to a temporal Gaussian profile. The beam mode structure was monitored during all experiments using a high-speed oscilloscope.

On exiting the cavity the laser beam first strikes a 2% reflecting wedge, which sends a fraction of the beam into the autocorrelator. The number of pulses striking the target is controlled by means of a computer controlled fast optical shutter, which has a rise and fall time of 5 ms. A repetition rate of 100Hz was used for all experiments. It was estimated that this repetition rate was sufficiently low enough to allow enough heat dissipation between successive pulses so that the initial temperature of the sample remained the same during consecutive pulses. The pulse energy was controlled using a combination of a rotary half-wave plate and a beam splitting polarizing cube. The pulse energy was measured using a pyroelectric detector placed just before the objective lens. The detector was used in conjunction with the manufacturers (Molelectron Inc.) software, which enabled the energy to be measured for 1000 consecutive pulses. This allowed for an average pulse energy and a corresponding standard deviation to be evaluated. An example of an energy readout showing the average and standard deviation as well as the Gaussian shaped distribution of energy values is shown in Fig. 3.

The beam passes through a pinhole of 3mm in diameter in order to achieve a more circular spot. A CCD camera image of the beam taken before the focus shows that the beam is almost circular (11% ellipticity) at this position, Fig. 2. It can also be seen from the image that the central part of the beam follows a Gaussian intensity distribution. At the edges of the beam, a diffraction pattern (caused by the pinhole) results in a deviation from the Gaussian distribution. In order to achieve a smaller focused spot the beam was expanded to twice its size by passing it through a 2x telescope. The focusing objective (120mm plano-convex lens) was mounted on a computer controlled z-axis translation stage, which was used to control the position of the focused beam relative to the targets, which were mounted perpendicular to the incident beam on a computer controlled x-y translation stage. The experimental arrangement is shown in Fig. 1.

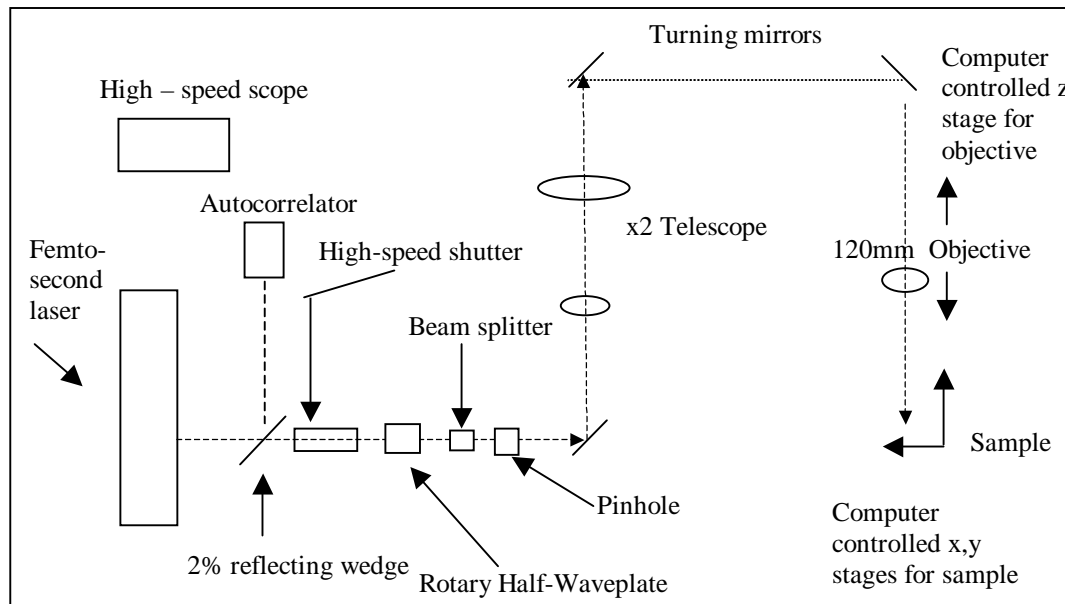


Fig. 1. Schematic of the experimental arrangement.

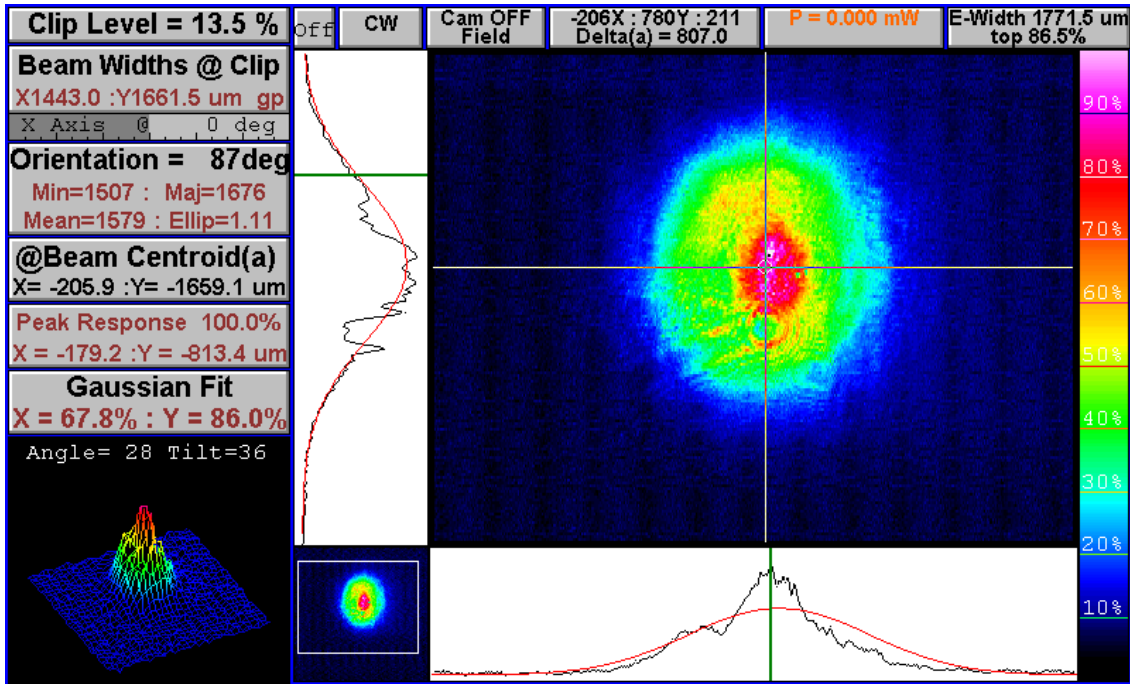


Fig. 2. CCD camera image of the laser beam taken before the focus.

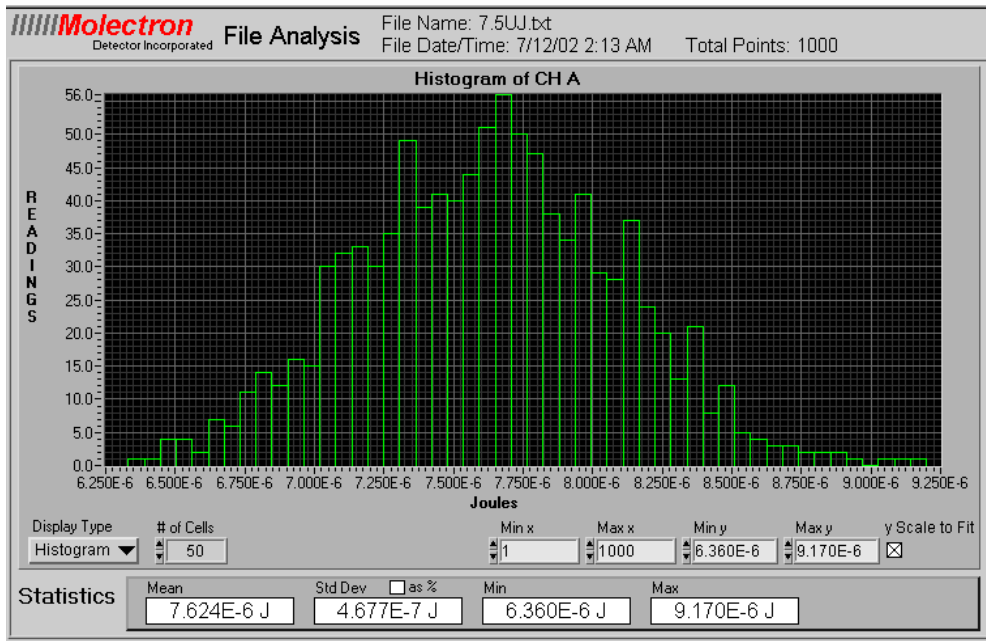


Fig. 3. An example of an energy readout showing the average and standard deviation values of the pulse energy as well as the Gaussian shaped distribution of energy values.

In order to get accurate measurements of crater depths and diameters a total of ten holes were produced at each value of laser fluence. All the holes were created using 100 laser shots. Using a white light scanning interferometer the diameter as well as the maximum depth of each hole was measured. Each value of depth and diameter obtained was thus an average of ten separate measurements and the error associated with the values was the standard deviation of these measurements. The values for the depth removed per pulse were obtained by dividing the depth values by the number of shots, i.e. 100.

### 3. RESULTS AND DISCUSSION

This section will be split into two parts. The first part will deal with the ablation threshold measurements and the second part will deal with the ablation rates of the metal studied.

#### 3.1 Ablation threshold measurements

The laser beam used in all of the experiments approximates to a Gaussian beam as can be seen from Fig. 2. As mentioned earlier there is a deviation of the intensity from the Gaussian distribution at the “edges” of the beam. The lateral precision of ablation depends on several laser and material related parameters. For laser ablation with a Gaussian spatial intensity beam profile a simple relation can be derived between the diameter,  $D$ , of an ablated crater and the material dependant surface damage threshold fluence ( $\phi_{th}$ ), the laser dependant Gaussian beam radius,  $\omega_0$  ( $1/e^2$ ), and the peak fluence in the beam,  $\phi_0$ .<sup>15,9</sup>

For a Gaussian beam, the spatial fluence profile,  $\phi(r)$ , is given by

$$\phi(r) = \phi_0 e^{-\frac{2r^2}{\omega_0^2}}, \quad (8)$$

where  $r$  is the distance from the beam centre and  $\omega_0$  and  $\phi_0$  are explained above. The peak fluence and the pulse energy,  $E_p$ , are directly related by

$$\phi_0 = \frac{2E_p}{\pi\omega_0^2}. \quad (9)$$

Finally it can be shown that for an ablation threshold fluence,  $\phi_{th}$ , the diameter,  $D$ , of an ablated crater is related to the peak fluence by

$$D^2 = 2\omega_0^2 \ln\left(\frac{\phi_0}{\phi_{th}}\right). \quad (10)$$

Because of the linear dependence of the peak laser fluence on the pulse energy it is possible to determine the beam radius,  $\omega_0$ , from a plot of the square of the crater diameters  $D^2$  versus the laser pulse energy,  $E_p$ . Once the beam radius is determined it is possible to convert the laser pulse energy,  $E_p$ , to the peak fluence in the beam using (9).

It is now possible to plot the squared diameters versus the peak laser fluence in the beam. By extrapolation of  $D^2$  back to zero a value for the ablation threshold fluence,  $\phi_{th}$ , can be obtained.

The method explained above has many distinct advantages over other methods. The most important of these being that a value for the Gaussian beam radius,  $\omega_0$ , can be easily obtained. This quantity is vital because it is necessary to always express pulse energies in terms of fluence rather than just as pulse energy. The fact that the method yields a value for the beam radius eliminates the need to measure the quantity which is notoriously difficult, unreliable and time consuming.

The use of peak rather than average laser fluence is useful also. If one considers the bell shaped intensity profile of a Gaussian laser beam there will be some instances where only the upper part of the energy distribution will be above the ablation threshold and so only this part of the beam will actually cause any ablation. Taking this into account it becomes clear why the peak fluence is a more meaningful quantity. The graphs obtained of  $D^2$  versus the natural logarithm of the peak laser fluence for the four metals used are presented in Fig. 4.

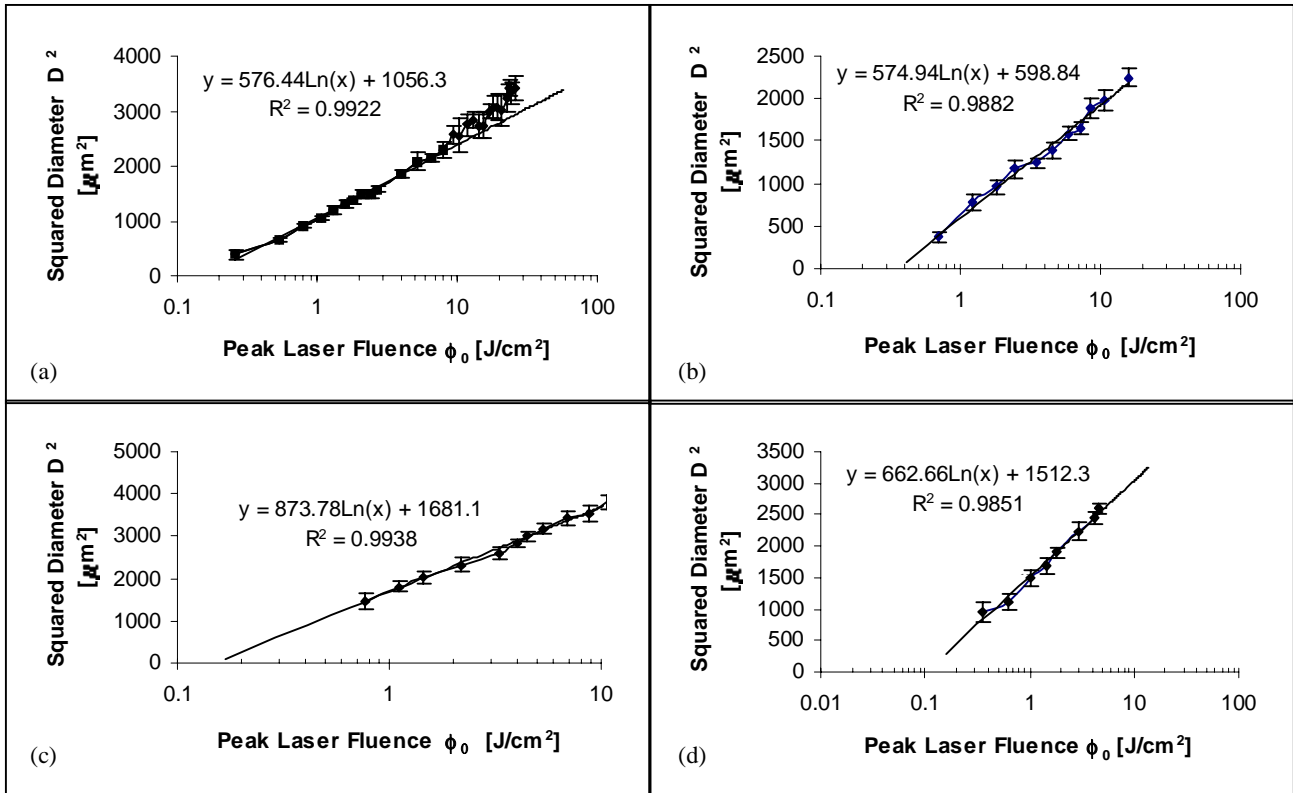


Fig. 4. : Results obtained for (a) stainless steel, (b) copper, (c) niobium and (d) titanium. The equations shown are of the least squares logarithmic fit to the data. The slopes of the lines were used to calculate the beam radius. The  $R^2$  value is a measure of how well the data fits. It is clear that each set of data fits very well.

There are some data points in Fig. 4(a) which clearly deviate from the straight line. It should be noted that these are high fluence values and the reason for this is the deviation of the beam intensity from the Gaussian distribution at the “edges” of the beam which was mentioned earlier. The “edges” of the beam begin to ablate at higher fluences. Therefore, only low-energy data points served as the basis for the theoretical fit in Fig. 4 (a). The high fluence data points were not used in the subsequent measurements on the other metals for this reason. The ablation threshold fluences for the metals used are presented in Table 1 shown below.

Metal	Ablation Threshold Fluence, $\phi_{th}$ . ( $\text{J}/\text{cm}^2$ )
Stainless Steel	0.1600
Copper	0.3529
Niobium	0.1460
Titanium	0.1021

Table 1. Ablation threshold values.

The values obtained for stainless steel, niobium and titanium show good agreement with results obtained for other metals,<sup>2</sup> whereas the value obtained for the ablation threshold of copper seems a little too high when compared to results obtained elsewhere.<sup>1,2</sup>

It should be noted that the above results are for a “multi-shot” ablation threshold fluence. It has been shown elsewhere<sup>9,13</sup> that there is a single-shot ablation threshold fluence, which is greater than the multi-shot threshold. The dependence of the ablation threshold on the number of laser shots indicates an incubation effect. However, this effect is more prominent when using semi-conductors and dielectrics and is virtually absent in metals.<sup>13</sup>

### 3.2 Ablation rate measurements

The results obtained for the ablated depth per pulse (DPP) versus the peak laser fluence for the metals used are shown in Fig. 5.

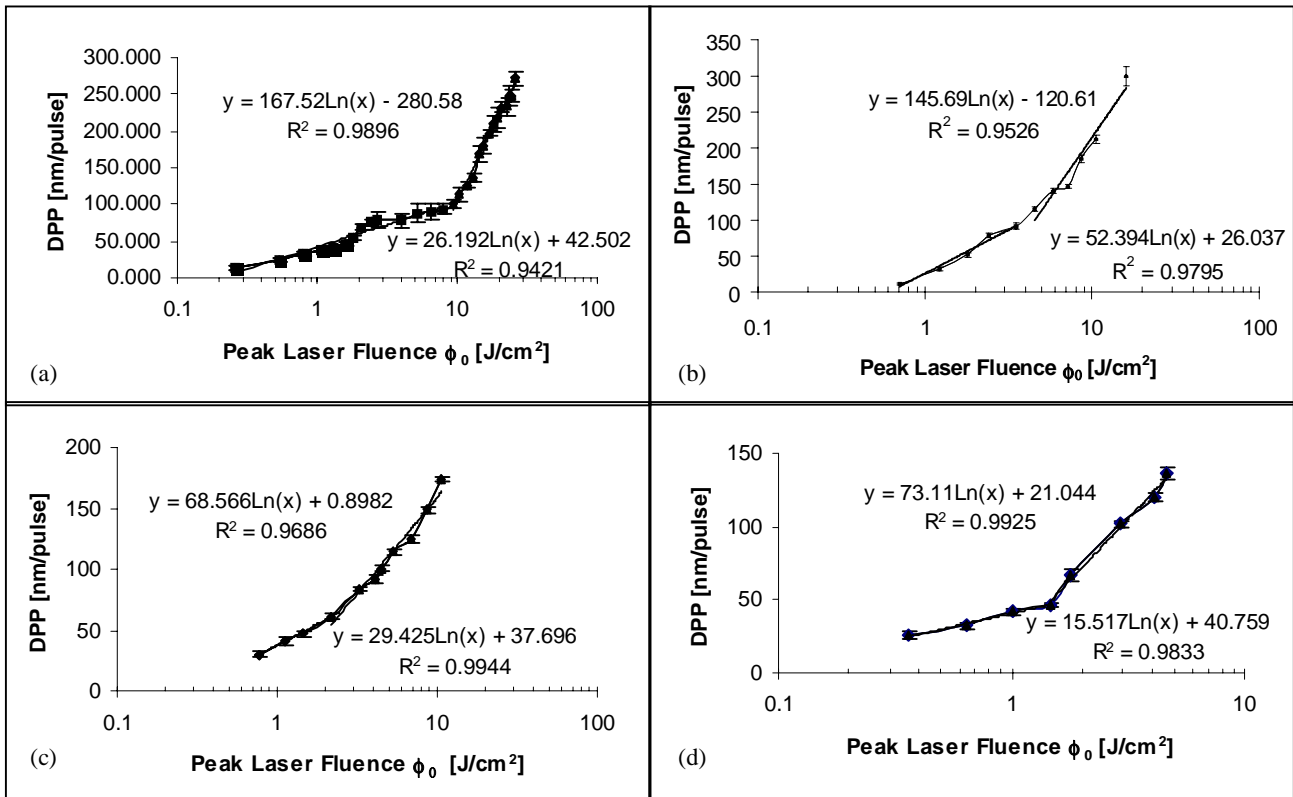


Fig. 5. : Results obtained for (a) stainless steel, (b) copper, (c) niobium and (d) titanium. There are two separate equations shown for each graph. These represent the least squares logarithmic fit to the data for the low and high fluence ablation regimes of each metal. Once again the  $R^2$  value is a measure of how well the data fits.

It is clear from the above data that there are two distinct ablation regimes governed by equations (3)

$[L \approx \alpha^{-1} \ln(\phi_0 / \phi_{th}^\alpha)]$  and (4)  $[L \approx l \ln(\phi_0 / \phi_{th}^l)]$  as explained in the introduction. In the first regime the ablation rate is low and is governed by the optical penetration depths of the metals involved. In the second regime the ablation rate is higher and is governed by the “electron heat diffusion length”,  $l$ , of each of the metals. The results obtained for copper Fig. 5(b) show good qualitative agreement to data obtained elsewhere.<sup>1</sup> The  $R^2$  values obtained for each regime and each metal show that the data points obtained fit very well to the logarithmic regimes apart from the low fluence regime in the case of stainless steel where there are some deviations. It should be noted that the fitted lines in themselves have no physical relevance and serve only to show that the data follows the logarithmic regimes (i.e. they are not the best fits of equations (3) and (4)).

For a more quantitative analysis to be carried out, a model would have to be constructed similar to the one used by Nolte et al<sup>1</sup>, and the data would have to be fitted to the equations which emerged from that model. This would yield values of the ablation threshold for the low and high fluence regimes as well as values for the optical penetration depths and “electron heat diffusion lengths” of each of the metals. However, in the case of evaluating ablation thresholds, it is believed that the method utilised in this paper is more reliable because of the difficulties involved in measuring the depths of small ( $\sim 30\mu\text{m}$  diameter) holes.

## 4. CONCLUSIONS

Measurements of the “multi-shot” ablation threshold fluence,  $\phi_{th}$ , have been carried out for stainless steel, copper, niobium and titanium using 150 fs laser pulses at a central wavelength of 775nm in air under atmospheric pressure. The results obtained (stainless steel: 0.1600 J/cm<sup>2</sup>, niobium: 0.1460 J/cm<sup>2</sup>, titanium: 0.1021 J/cm<sup>2</sup> and copper: 0.3529 J/cm<sup>2</sup>) show good agreement with results obtained elsewhere for similar metals.<sup>2</sup> The method used was shown to be reliable because of the degree to which the measured data agreed with the presented theory.

The existence of two separate ablation regimes with logarithmic relationships between the ablation rate and the laser fluence has been verified. In the low fluence ( $\phi_0 < 1 \text{ J/cm}^2$ ) regime the ablation rate is low and is characterized by the optical penetration depth of the metal. In the high fluence regime ( $\phi_0 > 1 \text{ J/cm}^2$ ) the ablation rate is higher and is characterized by the “electron heat diffusion length”. Good qualitative agreement has been obtained in the case of copper with work carried out by Nolte et al.<sup>1</sup> A source for comparison with the ablation rates obtained for the other metals has not been found. It is acknowledged that for a more complete treatment of the ablation process, a model will have to be constructed and fitted to the data. This would lead to experimentally obtained values for quantities such as the optical penetration depth and the “electron heat diffusion length” as well as an alternative method for finding the ablation threshold fluence.

## ACKNOWLEDGMENTS

This work was supported by the Higher Education Authority Program for Research in Third-Level Institutions (1999) and by the Enterprise Ireland PAT Research Program (2000).

## REFERENCES

- <sup>1</sup> S. Nolte, C. Momma, H. Jacobs, A. Tünnermann, B.N. Chichkov, B. Wellegehausen and H. Welling, “Ablation of metals by ultrashort laser pulses”, *J. Opt. Soc. Am. B* **14**, pp 2716-2722, 1997.
- <sup>2</sup> M. D. Shirk and P.A. Molian, “A review of ultrashort pulsed laser ablation materials”, *J. Laser Appl.* **10**, pp 18-28, 1998.
- <sup>3</sup> P.P. Pronko, S.K. Dutta, J. Squier, J.V. Rudd, D. Du and G. Mourou, “Machining of sub-micron holes using a femtosecond laser at 800 nm”, *Optics Comm.* **114**, pp 106-110, 1995.
- <sup>4</sup> X. Zhu, A.Yu. Naumov, D. M. Villeneuve and P.B. Corkum, “Influence of laser parameters and material properties on micro-drilling with femtosecond laser pulses”, *Appl. Phys. A*, **69**[Suppl.], pp S367-S371, 1999.
- <sup>5</sup> P.S. Banks, M.D. Feit, A.M. Rubenchik, B.C. Stuart and M.D. Perry, “Material effects in ultra-short pulse laser drilling of metals”, *Appl. Phys. A*, **69**[Suppl.], pp S377-S380, 1999.
- <sup>6</sup> J. Zhao, B. Huettner and Arnd Menschig, “Microablation with ultrashort laser pulses”, *Optics & Laser Technology* **33**, pp 487-491, 2001.
- <sup>7</sup> D. Bauerle *Laser Processing and Chemistry*, 2<sup>nd</sup> edn. ( Springer, Berlin, Heidelberg 1996 ).
- <sup>8</sup> B.N. Chichkov, C. Momma and S. Nolte, “Femtosecond, picosecond and nanosecond laser ablation of solids”, *Appl. Phys. A*, **63**, pp 134-142, 1996.
- <sup>9</sup> J. Bonse, J. M. Wrobel, J. Krüger and W. Kautek, “Ultrashort-pulse laser ablation of indium phosphide in air”, *Appl. Phys. A* **72**, pp 89-94, 2001.
- <sup>10</sup> W.S. Fann, R. Storz, H.W. Tom and J. Bokor, “Direct measurement of nonequilibrium electron-energy distributions in subpicosecond laser-heated gold films”, *Phys. Rev. Lett.* **68**, pp 2834-2837, 1992.
- <sup>11</sup> J. Hohlfeld, J.G. Müller, S.-S. Wellershoff and E. Matthias, “Time-resolved thermorefectivity of thin gold films and its dependence on film thickness”, *Appl. Phys. B*, **64**, pp 387-390, 1997.
- <sup>12</sup> K. Sokolowski-Tinten, A. Cavalleri and D. von der Linde, “Single-pulse time- and fluence-resolved optical measurements at femtosecond excited surfaces”, *Appl. Phys. A*, **69**, pp 577-579, 1999.
- <sup>13</sup> J. Güdde, J. Hohlfeld, J.G. Müller and E. Matthias, “Damage threshold dependence on electron-phonon coupling in Au and Ni films”, *Appl. Surface Science* **127-129**, pp 40-45, 1998.
- <sup>14</sup> M. Bonn, D. N. Denzler, S. Funk, M. Wolf, S.-S. Wellershoff and J. Hohlfeld, “Ultrafast electron dynamics at metal surfaces: Competition between electron-phonon coupling and hot-electron transport”, *Phys. Rev. B*, **61**, pp 1101-1105, 2000.
- <sup>15</sup> J.M. Liu, “Simple technique for measurement of pulsed Gaussian-beam spot sizes”, *Opt. Lett.* **7**, pp 196-198, 1982.